NANO LETTERS

pubs.acs.org/NanoLett

Letter

Mechanically Tunable Quantum Interference in Ferrocene-Based Single-Molecule Junctions

María Camarasa-Gómez,[#] Daniel Hernangómez-Pérez,[#] Michael S. Inkpen,[*] Giacomo Lovat, E-Dean Fung, Xavier Roy, Latha Venkataraman,[*] and Ferdinand Evers[*]

Cite This: *Nano Lett.* 2020, 20, 6381−6386

Read Online

ACCESS | Metrics & More | Article Recommendations | Supporting Information

ABSTRACT: Ferrocenes are ubiquitous organometallic building blocks that comprise a Fe atom sandwiched between two cyclopentadienyl (Cp) rings that rotate freely at room temperature. Of widespread interest in fundamental studies and real-world applications, they have also attracted some interest as functional elements of molecular-scale devices. Here we investigate the impact of the configurational degrees of freedom of a ferrocene derivative on its single-molecule junction conductance. Measurements indicate that the conductance of the ferrocene derivative, which is suppressed by 2 orders of magnitude as compared to a fully conjugated analogue, can be modulated by altering the junction configuration. *Ab initio* transport calculations show that the low conductance is a consequence of destructive quantum interference effects of the Fano type that arise from the hybridization of localized metal-based d-orbitals and the delocalized ligand-based π-system. By rotation of the Cp rings, the hybridization, and thus the quantum interference, can be mechanically controlled, resulting in a conductance modulation that is seen experimentally.

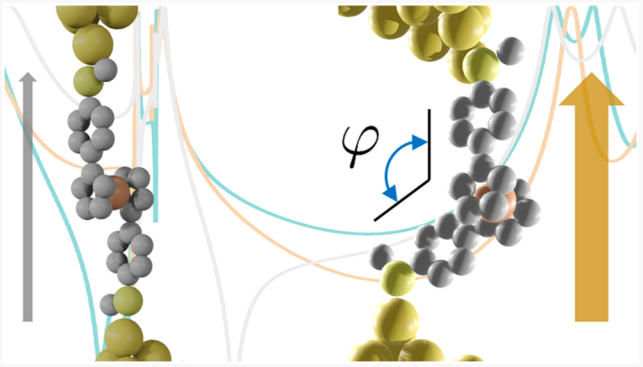

KEYWORDS: *single-molecule junctions, destructive quantum interference, d−π hybridization, ferrocene*

Metallocenes are archetypical organometallic compounds comprising a single metal atom sandwiched between two cyclopentadienyl (Cp) rings. Since the discovery of ferrocene in the 1950s[1,2] (metal atom = Fe), a variety of metallocenes and related sandwich organometallic structures have been synthesized and investigated.[3,4] One of the key features of ferrocene is that the barrier for the rotation of Cp rings is low (~0.05 eV).[5,6] The easy rotation provides flexibility for adsorption on metal surfaces, while also enabling ferrocene-based molecular wires to potentially adopt a range of geometries.[7] Remarkably, the impact of such conformational degrees on electron transport across ferrocene-based wires has not been demonstrated previously[8] despite their use as key elements of rectifiers,[9,10] switches,[11] or spin filters.[12,13] The consequences of the rotational flexibility of ferrocene on transport characteristics have only been computationally addressed recently.[14−18] Variations in the conductance by orders of magnitude have been predicted, which have been attributed to the sensitivity of the molecular geometry to the binding configuration[16] and/or to differences in Fermi level alignment of several molecular conformations in the junction.[15]

Here we undertake an experimental and theoretical study of coherent charge transport through single-branched ferrocene-based molecular junctions attached to gold electrodes. Using a series of model compounds, we find that single-molecule junctions comprising a ferrocene moiety present complex transport characteristics that can be attributed to quantum interference related to the metal-based d-orbitals. Our experiments show ferrocene derivatives have a lower conductance than a conjugated organic analogue of similar length while enabling a larger change of conductance upon mechanical modulation. Although mechanical tuning of quantum interference properties has been previously demonstrated for $\pi-\pi$ stacked dimers;[19,20] the rotational degree of freedom of ferrocene provides here a predefined mechanical deformation parameter that allows for controlled interference switching employing a Fano resonance. Our work also demonstrates the complexities of d-orbital-based interference effects that are not seen in any other carbon-based systems.

We study the conductance of two ferrocene derivatives consisting of a ferrocene unit terminated with two thioanisole gold-binding groups installed on the same (**1,3-Fe**) or opposite

Received: May 6, 2020
Revised: August 1, 2020
Published: August 3, 2020

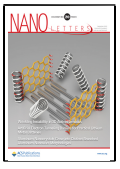

https://dx.doi.org/10.1021/acs.nanolett.0c01956
Nano Lett. 2020, 20, 6381−6386

(**1,1′-Fe**) Cp ring (Figure 1a). We measure their single-molecule conductance using the scanning tunneling micro-

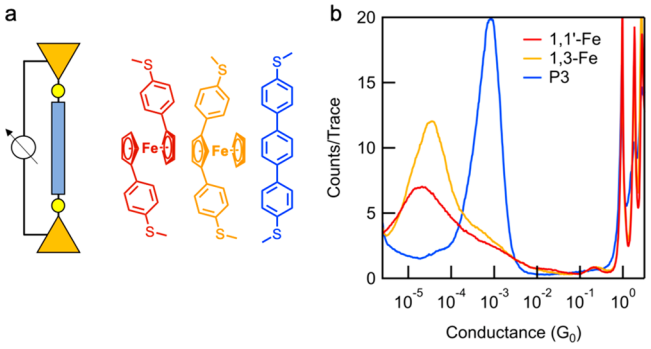

Figure 1. Molecule structures and conductance histograms. (a) Junction schematic and molecular structures of **1,1′-Fe** (red), **1,3-Fe** (orange), and **P3** (blue). (b) Logarithmically binned one-dimensional conductance histograms for **1,1′-Fe** (red), **1,3-Fe** (orange), and **P3** (blue) measurements. All histograms were built from 10 000 conductance traces without data selection measured at an applied bias of 450 mV.

scope (STM)-based break-junction technique[21,22] (see Methods for details) and compare the conductance features of the ferrocene derivatives to those of 4,4″-bis(methylthiol) *p*-terphenyl (**P3**, Figure 1a, blue schematic molecular structure). Figure 1b shows one-dimensional logarithmically binned conductance histograms created without data selection from 10 000 individual conductance-displacement traces. The conductances of **1,1′-Fe** and **1,3-Fe** are 2×10^{-5} G_0 and $3.3. \times 10^{-5}$ G_0, respectively, while the conductance of **P3** is 1×10^{-3} G_0 ($G_0 = 2e^2/h$, the conductance quantum). The two-dimensional conductance-displacement histograms clearly show that junctions of **P3** and **1,3-Fe** sustain the longest elongations while those of **1,1′-Fe** are the shortest (Figure S1). This accounts for the different conductance peak heights as also corroborated by a histogram of plateau lengths (Figure S2). Additionally, the ferrocene histogram peaks are broader near maximum and exhibit a tail that extends slightly beyond 10^{-3} G_0. We hypothesize that the conductance difference between **P3** and the ferrocene derivatives as well as the difference in the histogram peak widths result from the larger range of junction geometries sampled by the ferrocene junctions due to the easy rotation around the Cp rings.

To test this hypothesis, we calculated the electronic transmission for model molecular junctions with all three systems (see Methods and section III of the Supporting Information for the computational details). We show in Figure 2a two views of the optimized junction with **1,1′-Fe**. Analogous figures for **1,3-Fe** and **P3** are in Figure S3. We plot the energy-dependent transmission functions, $T(E)$, calculated at zero-bias for all three molecules in Figure 2b. Sharp antiresonances indicative of destructive interference are observed between the Fermi energy (E_F) and −1 eV for **1,3-Fe** and **1,1′-Fe** junctions, which suppress transmission around E_F. The origin of the antiresonances in both ferrocene-derived transmissions is similar, arising from a destructive interference from the Fano type. By contrast, the transmission function for **P3** shows clear evidence of constructive interference between the molecular HOMO and LUMO, yielding a much higher transmission around E_F. Focusing on **1,1′-Fe** junctions, we calculate its transmission for geometries with different relative

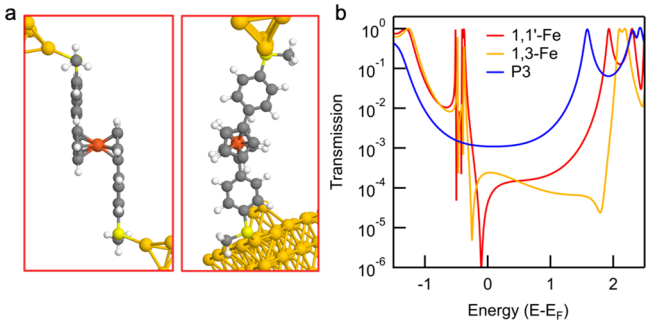

Figure 2. DFT-based calculations. (a) Optimized molecular junction structure for **1,1′-Fe** employed in the transport calculation. (b) Transmission functions for **1,1′-Fe** (red), **1,3-Fe** (orange), and **P3** (blue). Compared to **P3**, ferrocene-based transmissions show sharp antiresonances at around E_F, a signature of destructive quantum interference. By contrast, **P3** shows evidence of constructive interference (see ref 23. and Figure S7 in the Supporting Information), producing a significant increase of the conductance at E_F.

angle between the two Cp rings (see inset of Figure 3a and Figure S4 for the angle definition). The rotation occurs at low activation energy (see Figure S6 in the Supporting Information). Transmission curves calculated for geometries with three different angles are shown in Figure 3a. They clearly demonstrate that the antiresonance and its position can be controlled by rotating one ring relative to the other.

To follow this evolution more carefully, we calculate $T(E)$ for a series of angles and compile these into a two-dimensional plot (Figure 3b). The most prominent features are the blue regions corresponding to angular and energy intervals with strongly suppressed transmission (between 10^{-4} and 10^{-7}). The sharp yellow lines of high transmission ($>10^{-1}$) around −0.5 eV are resonances that are also seen in Figure 3a. We attribute these to weakly coupled localized, d-dominated molecular orbitals. At large angles ($\varphi > 120°$), the two thioanisole phenyl rings begin to overlap and a broader blue low transmission feature appears as a result of direct tunneling between the thioanisole groups, bypassing the ferrocene unit. This is detailed in Figure 3b, where we see that the presence or absence of destructive interferences can change the conductance at E_F by several orders of magnitude. Such geometries represent a very small S−S distance and present a large activation barrier (see Figure S6) and are highly unlikely to be probed in our experiments.

We analyze the contributions of the various orbitals of the system (molecule and electrode Au atoms) to the antiresonances for **1,1′-Fe**. In Figure 3c, we show states at energies corresponding to the HOMO−3, HOMO, and LUMO orbitals for the 30° structure (see Figure S8 for orbitals at other representative angles and additional details in Orbital symmetry analysis section of the Supporting Information). These orbitals, which have contributions from the Fe d-states with d_{yz}, $d_{x^2-y^2}$, and d_{xz} symmetries, are delocalized across the junctions as these d-states can couple to the Cp π-system. They give rise to the dominant transport resonances and participate in the rotation dependent quantum interference properties. By contrast, HOMO−2 (with d_{z2} symmetry) and HOMO−1 (d_{xy} symmetry) are strongly localized on the central ferrocene unit at all rotation angles because the overlap of hybridizing orbitals is small. They do not fit the nodal symmetry of the Cp π-system. These orbitals manifest in the

https://dx.doi.org/10.1021/acs.nanolett.0c01956
Nano Lett. 2020, 20, 6381−6386

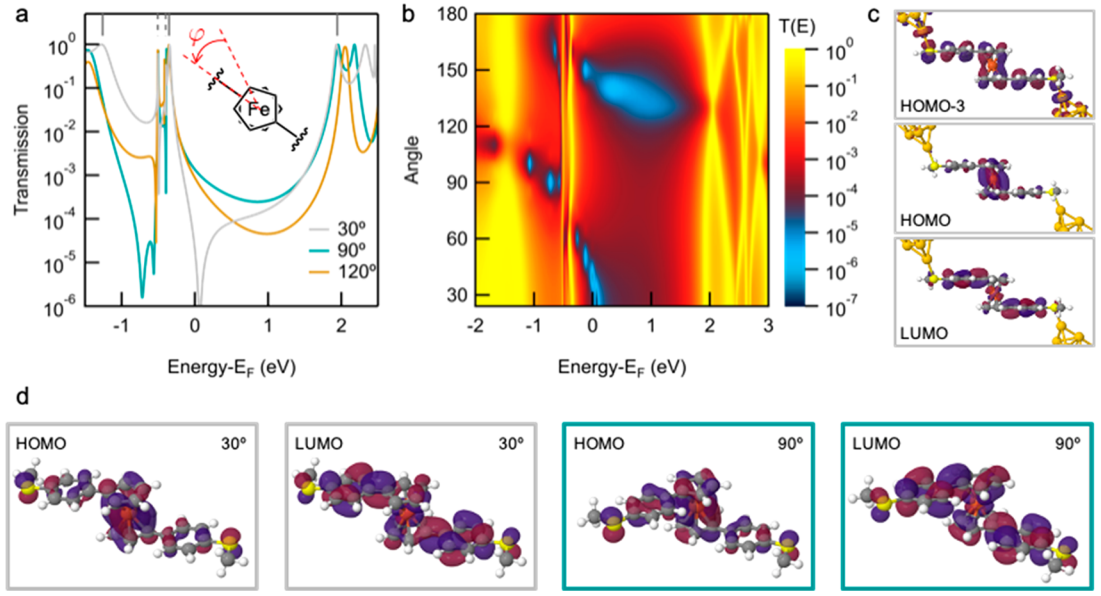

Figure 3. Transmission functions as a function of relative Cp ring angles for the **1,1′-Fe** junctions. (a) DFT-based transmission functions for **1,1′-Fe** model junctions at 30° (gray), 90° (green), and 120° (gold). For 30°, an antiresonance is seen between the HOMO and LUMO resonances. Coupled resonances (HOMO, HOMO−3, and LUMO) are marked by a solid bar on the top axis while the dashed bars mark the uncoupled HOMO−1 and HOMO−2 resonance. At 90°, the antiresonance shifts to lower energies (−0.8 eV). With an additional rotation of 30°, the interference is no longer destructive. Inset: Schematic illustrating angle definition; see Figure S4 for further details. (b). 2D-transmission map of **1,1′-Fe** junctions for angles between 24° and 180°. The areas associated with destructive quantum interference (blue) change with rotation. (c) Scattering states at HOMO−3, HOMO, and LUMO for the 30° **1,1′-Fe** junction. (d) Gas-phase HOMO and LUMO of **1,1′-Fe** for 30° and 90° angles. The nodal structure of the HOMO changes going from 30° to 90°.

transmission as sharp resonances between 24° and 120° discussed above.

In order to explain how rotating the Cp rings modifies interferences, we generalize a perspective formulated by previous authors;[24] moreover, our results include but are not limited to carbon-based molecules[25−30] or simple ("toy") models.[31] Our argument embarks on the familiar trace formula for the transmission $T(E) = \mathrm{Tr}(\Gamma_L G \Gamma_R G^+)$.[32] It expresses $T(E)$ as the product of two Greens functions, $G(E)$ which are sums of a series of poles, where each pole represents a molecular orbital.[33] We thus have a representation

$$T(E) = \sum_i T_i + \sum_{i \neq j} T_{ij} \tag{1}$$

The first term in eq 1 sums the single-pole contributions which are well parametrized as Lorentzians

$$T_i(E) = \frac{\gamma_{iL}\gamma_{iR}}{(E - \varepsilon_i)^2 + \gamma_i^2} \tag{2}$$

where $\gamma_{i\{L,R\}}$ denotes the broadening resulting from the coupling of the ith orbital to left/right electrodes and $\gamma_i = (\gamma_{iL} + \gamma_{iR})/2$. The second term in eq 1 includes the mixed terms of the product, i.e., the interference terms, which are effectively

$$T_{ij}(E) \cong -2 \cos \psi_{ij} |T_i(E)|^{1/2} |T_j(E)|^{1/2} \tag{3}$$

The angle ψ_{ij} accounts for the relative phase of the tunneling wave across the orbitals i and j. For well separated resonances, $\gamma_i, \gamma_j \ll |E_i - E_j|$, $T_{ij}(E)$ is small irrespective of the type of molecule considered. When $\psi_{ij} = \pi$, interference is constructive, while at $\psi_{ij} = 0$, it is destructive if $E_i < E < E_j$.[24] Importantly, the relative phase ψ_{ij} is a property inherent to the molecule and thus can be inferred by looking at the molecular orbitals of the isolated molecule as long as the orbitals do not reorder when the molecule is coupled to the electrodes. Indeed, for the molecule with Cp rings at 30° relative angle, the amplitude of both the HOMO and LUMO on the left and right S atom have the opposite sign; hence, the relative shift vanishes, $\psi_{ij} \sim 0$ and the interference is destructive (Figure 3d). For a 90° relative angle, the amplitude of the HOMO is the same on each S atom, making the relative phase-shift $\psi_{ij} \approx \pi$. The interference is constructive and leads to a transmission with no antiresonance between the HOMO and LUMO resonances, as observed in Figure 3a. Similar analyses can be made with other pairs of orbitals. For example, HOMO and HOMO−3 show evidence of constructive interference in the 30° junction for an energy range between the two orbitals.

To experimentally demonstrate this variation in transmission with the rotation angle, we carry out modified STM-BJ experiments with **1,1′-Fe** where we first form a molecular junction, then modulate the tip−sample separation with an amplitude of 2.4 Å while measuring the conductance (Figure 4a). The distance of 2.4 Å was chosen as this is close to the change in the calculated junction length going from 30° to 90°. In Figure 4b, we overlay all traces that form and sustain a molecular junction during the modulation in a two-dimensional histogram (1900 out of 4300 traces). We find that as the tip−sample separation decreases, the junction conductance increases significantly. The inset of Figure 4b shows line profiles comparing the conductances when the junctions are pushed together or pulled apart during the first hold segment. The conductance increases on average by a factor of 6.7 when pushed together by 2.4 Å. By contrast, when the same experiment is performed with **P3**, the conductance increases by a factor of only 2.6. Although the highest conductance measured for **1,1′-Fe** is still lower than that of **P3**, the fact that the conductance for **1,1′-Fe** has a higher modulation ratio

https://dx.doi.org/10.1021/acs.nanolett.0c01956
Nano Lett. 2020, 20, 6381−6386

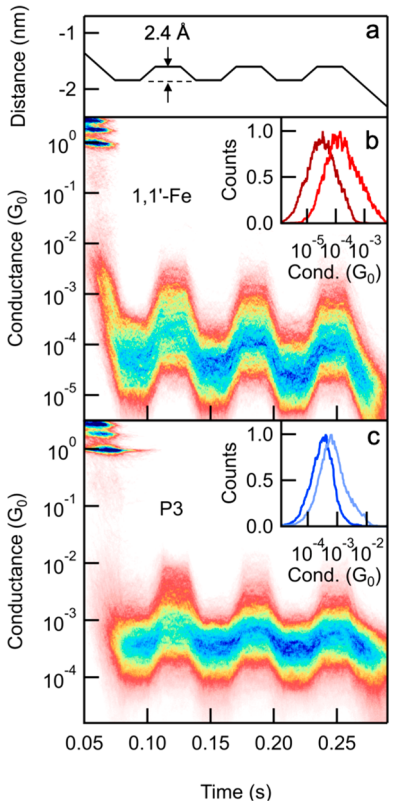

Figure 4. Modulation of the tip/sample separation in **1,1′-Fe** and **P3** junctions. (a) Piezo displacement as a function of time showing the modulation of the tip/substrate gap. (b) 2D histogram of **1,1′-Fe** traces obtained during tip/sample modulation. The conductance of the junction increases (decreases) when the distance between tip and sample is decreased (increased). The conductance changes by a factor of ∼7 upon modulation. Inset: Line-profiles taken at ∼0.09 s (dark) and 0.12 s (light) comparing the conductance between the maximal and minimal elongation point. (c) Analogous data for **P3** showing that the conductance increase upon modulation is only a factor ∼3.

with changing distance strongly supports that the **1,1′-Fe** junctions are conformationally more flexible and that such conformational changes have a greater influence on **1,1′-Fe** junction conductance. We briefly discuss alternative effects that are also known to induce conductance variations. First, the linker-metal contact can reorganize,[34,35] especially due to the flexibility of the thiomethyl end group. We do not believe this effect to dominate the difference in the modulation observed experimentally between **1,1′-Fe** and **P3** molecular junctions because both molecules have the same linker. Second, the conductance can be modulated because the gap between the electrodes is changed upon elongation and compression of the junction.[35,36] Therefore, the through-space contribution to the conductance is altered. This would also result in roughly the same change for both molecules as the experimental protocol applied is the same in both measurements. Third, the difference in the modulation could be due to changes in the molecular conformation induced by the mechanical modulation.[19,20,36,37] We believe this effect to be dominant in **1,1′-Fe** but much weaker in **P3**. On the basis of our *ab initio* and model calculations, we interpret the conductance oscillations as resulting from changes in the interference properties upon Cp ring rotation in the **1,1′-Fe** molecule.

We have shown that molecular junctions comprising ferrocene derivatives with different substitution patterns exhibit destructive quantum interference effects produced by the interplay of several localized and delocalized orbitals. These interferences determine the transmission characteristics and decrease the low-bias conductance while allowing the conductance to be changed by modulating the electrode separation. Our single-molecule conductance measurements are corroborated by theoretical transmission computations showing how interference features of the ferrocene derivative (from destructive to constructive) evolve when the Cp rings rotate relative to one another, a low-energy conformational degree of freedom inherent to ferrocene.

METHODS

STM-BJ Measurements. We measure the single-molecule conductance using the STM-BJ technique with a custom-built setup described previously.[22] Briefly, we drive a Au tip in and out of contact with a Au-substrate and record the junction's conductance as the tip is withdrawn. Upon rupture of the Au contact, a molecule may bridge the gap as evidenced by an additional plateau in the conductance versus displacement trace. We collect 10 000 such traces, which contain 2000 data points per nanometer of extension (40 kHz sampling rate) and construct the (normalized) 1D and 2D conductance histograms without data selection. All ferrocene derivatives studied here were introduced into the setup in a tetradecane solution with 0.1−1 mM concentration while **P3** was studied from a 1,2,4-trichlorobenzene solution.

DFT Calculations. Molecular junctions consist of molecules bound to pyramidal Au electrodes; geometries are optimized using density functional theory employing FHI-aims[38] with PBE functional.[39] Transport computations use DFT with the nonequilibrium Green's function formalism (NEGF) as implemented in the package AITRANSS;[40,41] for details, see section III in the Supporting Information.

ASSOCIATED CONTENT

Supporting Information

The Supporting Information is available free of charge at https://pubs.acs.org/doi/10.1021/acs.nanolett.0c01956.

Synthetic details, STM-BJ measurements and *ab initio* calculation details, additional data (two-dimensional conductance histograms, optimized junction geometries, definition of the relative angles as referred to in the main text, energetics of ring rotation in isolated **1,1′-Fe**, isosurface plots of the relevant Kohn−Sham orbitals of the **1,1′-Fe** junction, model interference properties of **P3**), additional discussion of the d-orbital symmetry and bonding in **1,1′-Fe**, and NMR spectra (PDF)

AUTHOR INFORMATION

Corresponding Authors

Michael S. Inkpen − *Department of Applied Physics and Applied Mathematics, Columbia University, New York, New York 10027, United States;* orcid.org/0000-0001-7339-8812; Email: inkpen@usc.edu

Latha Venkataraman − *Department of Applied Physics and Applied Mathematics and Department of Chemistry, Columbia University, New York, New York 10027, United States;* orcid.org/0000-0002-6957-6089; Email: lv2117@columbia.edu

https://dx.doi.org/10.1021/acs.nanolett.0c01956
Nano Lett. 2020, 20, 6381−6386

Ferdinand Evers − *Institute of Theoretical Physics, University of Regensburg, 93040 Regensburg, Germany*; Email: ferdinand.evers@ur.de

Authors

María Camarasa-Gómez − *Institute of Theoretical Physics, University of Regensburg, 93040 Regensburg, Germany*

Daniel Hernangómez-Pérez − *Institute of Theoretical Physics, University of Regensburg, 93040 Regensburg, Germany; Department of Materials and Interfaces, Weizmann Institute of Science, Rehovot 761001, Israel;* orcid.org/0000-0002-4277-0236

Giacomo Lovat − *Department of Applied Physics and Applied Mathematics, Columbia University, New York, New York 10027, United States*

E-Dean Fung − *Department of Applied Physics and Applied Mathematics, Columbia University, New York, New York 10027, United States;* orcid.org/0000-0001-6996-0243

Xavier Roy − *Department of Chemistry, Columbia University, New York, New York 10027, United States;* orcid.org/0000-0002-8850-0725

Complete contact information is available at: https://pubs.acs.org/10.1021/acs.nanolett.0c01956

Author Contributions

#M.C.-G. and D.H.-P. made equal contributions.

Notes

The authors declare no competing financial interest.

■ ACKNOWLEDGMENTS

M.C.-G. and D.H.-P. thank R. Korytár for discussions. M.C.-G., D.H.-P. and F.E. acknowledge financial support from the German Research Foundation (DFG) through Research Training Group (GRK) 1570 and Collaborative Research Center (SFB) 1277 − Project ID 314695032 (subprojects A03, B01). L.V., X.R., and G. L. acknowledge support by the Center for Precision Assembly of Superstratic and Superatomic Solids at Columbia University, an NSF MRSEC (award number DMR-1420634) and by NSF CHE-1807654. M.S.I. was supported by a Marie Skłodowska Curie Global Fellowship (MOLCLICK: 657247) within the Horizon 2020 Programme.

■ REFERENCES

(1) Kealy, T. J.; Pauson, P. L. A New Type of Organo-Iron Compound. *Nature* **1951**, *168*, 1039−1040.
(2) Miller, S. A.; Tebboth, J. A.; Tremaine, J. F. 114. Dicyclopentadienyliron. *J. Chem. Soc.* **1952**, 632−635.
(3) Astruc, D. Why is Ferrocene so Exceptional? *Eur. J. Inorg. Chem.* **2017**, *2017*, 6−29.
(4) Togni, A.; Hayashi, T. *Ferrocenes: Homogeneous Catalysis, Organic Synthesis*: Materials Science. Wiley-VCH: Weinheim, 1995.
(5) Haaland, A.; Nilsson, J.-E. The determination of the barrier to internal rotation in ferrocene and ruthenocene by means of electron diffraction. *Chem. Commun. (London)* **1968**, 88.
(6) Abel, E. W.; Long, N. J.; Orrell, K. G.; Osborne, A. G.; Šik, V. Dynamic NMR studies of ring rotation in substituted ferrocenes and ruthenocenes. *J. Organomet. Chem.* **1991**, *403*, 195−208.
(7) Vollmann, M.; Butenschön, H. Synthesis of a functionalized dialkynylferrocene for molecular electronics. *C. R. Chim.* **2005**, *8*, 1282−1285.
(8) Getty, S. A.; Engtrakul, C.; Wang, L.; Liu, R.; Ke, S.-H.; Baranger, H. U.; Yang, W.; Fuhrer, M. S.; Sita, L. R. Near-perfect conduction through a ferrocene-based molecular wire. *Phys. Rev. B: Condens. Matter Mater. Phys.* **2005**, *71*, 241401.
(9) Nijhuis, C. A.; Reus, W. F.; Whitesides, G. M. Mechanism of Rectification in Tunneling Junctions Based on Molecules with Asymmetric Potential Drops. *J. Am. Chem. Soc.* **2010**, *132*, 18386−18401.
(10) Matsuura, Y. Current rectification in nickelocenylferrocene sandwiched between two gold electrodes. *J. Chem. Phys.* **2013**, *138*, No. 014311.
(11) Liu, R.; Ke, S.-H.; Yang, W.; Baranger, H. U. Cobaltocene as a spin filter. *J. Chem. Phys.* **2007**, *127*, 141104.
(12) Zhou, L.; Yang, S.-W.; Ng, M.-F.; Sullivan, M. B.; Tan Shen, L. One-Dimensional Iron−Cyclopentadienyl Sandwich Molecular Wire with Half Metallic, Negative Differential Resistance and High-Spin Filter Efficiency Properties. *J. Am. Chem. Soc.* **2008**, *130*, 4023−4027.
(13) Pal, A. N.; Li, D.; Sarkar, S.; Chakrabarti, S.; Vilan, A.; Kronik, L.; Smogunov, A.; Tal, O. Nonmagnetic single-molecule spin-filter based on quantum interference. *Nat. Commun.* **2019**, *10*, 5565.
(14) Zhao, X.; Kastlunger, G.; Stadler, R. Quantum interference in coherent tunneling through branched molecular junctions containing ferrocene centers. *Phys. Rev. B: Condens. Matter Mater. Phys.* **2017**, *96*, 085421.
(15) Zhao, X.; Stadler, R. DFT-based study of electron transport through ferrocene compounds with different anchor groups in different adsorption configurations of an STM setup. *Phys. Rev. B: Condens. Matter Mater. Phys.* **2019**, *99*, No. 045431.
(16) Kanthasamy, K.; Ring, M.; Nettelroth, D.; Tegenkamp, C.; Butenschön, H.; Pauly, F.; Pfnür, H. Charge Transport through Ferrocene 1,1′-Diamine Single-Molecule Junctions. *Small* **2016**, *12*, 4849−4856.
(17) Bredow, T.; Tegenkamp, C.; Pfnür, H.; Meyer, J.; Maslyuk, V. V.; Mertig, I. Ferrocene-1,1′-dithiol as molecular wire between Ag electrodes: The role of surface defects. *J. Chem. Phys.* **2008**, *128*, No. 064704.
(18) Morari, C.; Rungger, I.; Rocha, A. R.; Sanvito, S.; Melinte, S.; Rignanese, G.-M. Electronic Transport Properties of 1,1′-Ferrocene Dicarboxylic Acid Linked to Al(111) Electrodes. *ACS Nano* **2009**, *3*, 4137−4143.
(19) Stefani, D.; Weiland, K. J.; Skripnik, M.; Hsu, C.; Perrin, M. L.; Mayor, M.; Pauly, F.; van der Zant, H. S. J. Large Conductance Variations in a Mechanosensitive Single-Molecule Junction. *Nano Lett.* **2018**, *18*, 5981−5988.
(20) Frisenda, R.; Janssen, V. A. E. C.; Grozema, F. C.; van der Zant, H. S. J.; Renaud, N. Mechanically controlled quantum interference in individual π-stacked dimers. *Nat. Chem.* **2016**, *8*, 1099−1104.
(21) Xu, B. Q.; Tao, N. J. Measurement of single-molecule resistance by repeated formation of molecular junctions. *Science* **2003**, *301*, 1221−1223.
(22) Venkataraman, L.; Klare, J. E.; Tam, I. W.; Nuckolls, C.; Hybertsen, M. S.; Steigerwald, M. L. Single-Molecule Circuits with Well-Defined Molecular Conductance. *Nano Lett.* **2006**, *6*, 458−462.
(23) Li, Y.; Buerkle, M.; Li, G.; Rostamian, A.; Wang, H.; Wang, Z.; Bowler, D. R.; Miyazaki, T.; Xiang, L.; Asai, Y.; Zhou, G.; Tao, N. Gate controlling of quantum interference and direct observation of anti-resonances in single molecule charge transport. *Nat. Mater.* **2019**, *18*, 357−363.
(24) Géranton, G.; Seiler, C.; Bagrets, A.; Venkataraman, L.; Evers, F. Transport properties of individual C60-molecules. *J. Chem. Phys.* **2013**, *139*, 234701.
(25) Yoshizawa, K.; Tada, T.; Staykov, A. Orbital Views of the Electron Transport in Molecular Devices. *J. Am. Chem. Soc.* **2008**, *130*, 9406−9413.
(26) Taniguchi, M.; Tsutsui, M.; Mogi, R.; Sugawara, T.; Tsuji, Y.; Yoshizawa, K.; Kawai, T. Dependence of Single-Molecule Conductance on Molecule Junction Symmetry. *J. Am. Chem. Soc.* **2011**, *133*, 11426−11429.
(27) Datta, S.; Melloch, M. R.; Bandyopadhyay, S.; Noren, R.; Vaziri, M.; Miller, M.; Reifenberger, R. Novel Interference Effects between Parallel Quantum Wells. *Phys. Rev. Lett.* **1985**, *55*, 2344−2347.

(28) Solomon, G. C.; Andrews, D. Q.; Hansen, T.; Goldsmith, R. H.; Wasielewski, M. R.; Van Duyne, R. P.; Ratner, M. A. Understanding quantum interference in coherent molecular conduction. *J. Chem. Phys.* **2008**, *129*, 054701.
(29) Gunasekaran, S.; Greenwald, J. E.; Venkataraman, L. Visualizing Quantum Interference in Molecular Junctions. *Nano Lett.* **2020**, *20*, 2843.
(30) Yoshizawa, K. An Orbital Rule for Electron Transport in Molecules. *Acc. Chem. Res.* **2012**, *45*, 1612−1621.
(31) Lambert, C. J. Basic concepts of quantum interference and electron transport in single-molecule electronics. *Chem. Soc. Rev.* **2015**, *44*, 875−888.
(32) Jauho, A. P.; Wingreen, N. S.; Meir, Y. Time-dependent transport in interacting and noninteracting resonant-tunneling systems. *Phys. Rev. B: Condens. Matter Mater. Phys.* **1994**, *50*, 5528−5544.
(33) Evers, F.; Korytár, R.; Tewari, S.; van Ruitenbeek, J. M. Advances and challenges in single-molecule electron transport. *Rev. Mod. Phys.* **2020**, *92*, No. 035001.
(34) Zhou, J.; Guo, C.; Xu, B. Electron transport properties of single molecular junctions under mechanical modulations. *J. Phys.: Condens. Matter* **2012**, *24*, 164209.
(35) Quek, S. Y.; Kamenetska, M.; Steigerwald, M. L.; Choi, H. J.; Louie, S. G.; Hybertsen, M. S.; Neaton, J. B.; Venkataraman, L. Mechanically controlled binary conductance switching of a single-molecule junction. *Nat. Nanotechnol.* **2009**, *4*, 230−234.
(36) Mejía, L.; Renaud, N.; Franco, I. Signatures of Conformational Dynamics and Electrode-Molecule Interactions in the Conductance Profile During Pulling of Single-Molecule Junctions. *J. Phys. Chem. Lett.* **2018**, *9*, 745−750.
(37) Pirrotta, A.; De Vico, L.; Solomon, G. C.; Franco, I. Single-molecule force-conductance spectroscopy of hydrogen-bonded complexes. *J. Chem. Phys.* **2017**, *146*, No. 092329.
(38) Blum, V.; Gehrke, R.; Hanke, F.; Havu, P.; Havu, V.; Ren, X.; Reuter, K.; Scheffler, M. Ab initio molecular simulations with numeric atom-centered orbitals. *Comput. Phys. Commun.* **2009**, *180*, 2175−2196.
(39) Perdew, J. P.; Burke, K.; Ernzerhof, M. Generalized Gradient Approximation Made Simple. *Phys. Rev. Lett.* **1996**, *77*, 3865−3868.
(40) Arnold, A.; Weigend, F.; Evers, F. Quantum chemistry calculations for molecules coupled to reservoirs: Formalism, implementation, and application to benzenedithiol. *J. Chem. Phys.* **2007**, *126*, 174101.
(41) Bagrets, A. Spin-Polarized Electron Transport Across Metal−Organic Molecules: A Density Functional Theory Approach. *J. Chem. Theory Comput.* **2013**, *9*, 2801−2815.

https://dx.doi.org/10.1021/acs.nanolett.0c01956
Nano Lett. 2020, 20, 6381−6386